The Astrophysical Journal, 1002:206 (7pp), 2026 May 10 https://doi.org/10.3847/1538-4357/ae5a9b

Supernova Dust Synthesis—Carbonaceous Dust in the Very Early Universe

Gen Chiaki[1,2], Chiaki Kobayashi[3], and Nozomu Tominaga[2,4,5]
[1] Department of Social Design Engineering, National Institute of Technology (KOSEN), Kochi College, 200-1 Monobe Otsu, Nankoku, Kochi, 783-8508, Japan
[2] Division of Science, National Astronomical Observatory of Japan, 2-21-1 Osawa, Mitaka, Tokyo 181-8588, Japan
[3] Centre for Astrophysics Research, Department of Physics, Astronomy and Mathematics, University of Hertfordshire, Hatfield, AL10 9AB, UK
[4] Department of Astronomical Science, SOKENDAI (The Graduate University for Advanced Studies), Osawa 2-21-1, Mitaka, Tokyo, 181-8588, Japan
[5] Department of Physics, Faculty of Science and Engineering, Konan University, 8-9-1 Okamoto, Kobe, Hyogo 658-8501, Japan
Received 2025 June 16; revised 2026 January 21; accepted 2026 February 17; published 2026 May 7

Abstract

Recent observations have revealed the spectral features of carbonaceous grains even in very distant galaxies. We develop a state-of-the-art dust synthesis code by self-consistently solving molecule and dust formation in supernova (SN) ejecta that contain various elements in different layers. With a progenitor mass $25\,M_{\odot}$ and explosion energy 10^{52} erg, we run the following four test calculations to investigate the impact of input physics. (i) With molecule formation solved, our SN model produces $8.45 \times 10^{-2}\,M_{\odot}$ carbonaceous grains. (ii) If all available C and Si were initially depleted into CO and SiO molecules, respectively, the C grain mass could be underestimated by ∼40%. In these two models producing $0.07\,M_{\odot}^{56}$ Ni without mixing fallback, a large amount of silicates ($0.260\,M_{\odot}$) created in O-rich layers are also ejected and likely to hide the spectral feature of carbonaceous grains. We then consider mixing fallback that can reproduce the observed elemental abundance ratios of C-normal and C-enhanced extremely metal-poor stars in the Milky Way. (iii) In the former, the mass ratio of carbonaceous to silicate grains is still small (∼0.3). However, (iv) in the latter (known as a "faint SN"), while the C grain mass is unchanged ($6.78 \times 10^{-2}\,M_{\odot}$), the silicate mass is reduced ($9.98 \times 10^{-3}\,M_{\odot}$). Therefore, we conclude that faint supernovae could be significant carbonaceous dust factories in the early Universe.

Unified Astronomy Thesaurus concepts: Dust formation (2269); Early universe (435); Population III stars (1285); Supernovae (1668); High-redshift galaxies (734)

1. Introduction

Long-term observational campaigns with the Herschel Space Observatory and the Atacama Large Millimeter Array (ALMA) have revealed that high-redshift galaxies ($z \sim 8$) contain dust grains—the condensates of metallic nuclei—with a mass of $\sim 10^8\,M_{\odot}$, corresponding to a dust to stellar mass ratio of ∼1%. It is puzzling how these galaxies have acquired such a large amount of grains for the short time, ∼600 Myr, since the Big Bang (D. Watson et al. 2015; Y. Tamura et al. 2019; P. Dayal et al. 2022; J. Witstok et al. 2022). In addition, the James Webb Space Telescope (JWST) has opened a new window to observe the galactic chemical and dust evolution (GCE) in the very early Universe (e.g., A. J. Bunker et al. 2023; F. D'Eugenio et al. 2023; J. Witstok et al. 2023a; S. Carniani et al. 2024).

With the NIRSpec instrument on the JWST, J. Witstok et al. (2023b) found the spectroscopic feature of carbonaceous (C) grains known as a "UV bump" in the galaxy, JADES-GS-z6-0, at redshift $z = 6.7$. In such a distant galaxy, the origin of C grains is unknown; since there is no time for low-mass stars to contribute to the dust formation, core-collapse supernovae (SNe) from the first generation of metal-free (Population III or "Pop III") stars are likely to be the major dust source (P. Todini & A. Ferrara 2001; T. Nozawa et al. 2003; R. Schneider et al. 2003). However, it has been considered that SNe mainly produce another species, silicates, because SN ejecta is oxygen-rich in most cases (S. Bianchi & R. Schneider 2007; A. Sarangi & I. Cherchneff 2015; S. Marassi et al. 2019). Unless the C grain mass is comparable to or more than the silicate grain mass, the remarkable UV bump cannot appear (T. Nozawa & M. Fukugita 2013). A more sophisticated dust formation model is required in order to predict the mass of each grain species in detail.

In this paper, based on the previous work (T. Nozawa & T. Kozasa 2013, N13), we revisit dust formation in Pop III SNe, developing a state-of-the-art dust synthesis code with all relevant physical processes: hydrodynamics, explosive nucleosynthesis, radiative transfer, nuclear decays, self-consistent molecule formation, and ejection with mixing/fallback. First, our code starts with pre-SN stars calculated by H. Umeda et al. (2000) with their stellar evolution code. Then, we calculate explosive nucleosynthesis (N. Tominaga et al. 2007). It is important to note that these have also been used to calculate our nucleosynthesis yields for the Galactic chemical evolution in C. Kobayashi et al. (2006, 2020) as well as for the Galactic archeology studies in N. Tominaga et al. (2014) and M. N. Ishigaki et al. (2018). These works found a significant contribution of supernovae with explosion energies of $\geqslant 10^{52}$ erg, known as hypernovae.

The pre-SN stars have an "onion-like structure," where lighter elements lie in outer layers. Hence, C grains and silicates are expected to mainly form in outer and intermediate layers of ejecta, respectively. If the chemical composition of SN ejecta is fully mixed, a significant amount of C atoms would be oxidized into CO molecules, which can suppress C grain formation as pointed out by S. Marassi et al. (2014). Therefore, we calculate dust formation while keeping the radial structure of SN ejecta.

Finally, we consider molecule formation that can compete with dust formation (S. Marassi et al. 2014, 2015).[6] For example, in the inner part of the C layer, oxygen is also synthesized. If C atoms are completely depleted into CO molecules, there are no longer C atoms available for forming C grains. Similarly, metallic silicon (Si) grains form in Si-rich layers, where sulfur is also abundant, and thus SiS molecules can suppress Si grain formation. S. Marassi et al. (2015) did not consider SiS molecule formation. N13 considered both, but in their model, all C and Si atoms were assumed to be initially depleted into CO and SiO molecules, respectively, for simplicity. This setup might lead to underestimation of C grain mass and overestimation of Si grain mass. To overcome this problem, we here calculate huge chemical networks of not only grain formation but also molecule formation (Section 2).

Most earlier works have considered an SN model with a "mass cut" that yields a constant ^{56}Ni mass of $M_{^{56}\mathrm{Ni}} = 0.07\,M_\odot$ (N13, C. Biscaro & I. Cherchneff 2014). This value was chosen to reproduce the observed light curve of SN 1987A and is not necessarily applicable to Pop III SNe. Although Pop III SNe have not been directly observed yet, their properties have been constrained from the observed elemental abundances of extremely metal-poor (EMP) stars, defined via their iron abundances [Fe/H] < -3 (M. N. Ishigaki et al. 2018; A. Choplin et al. 2019);[7] EMP stars are considered to form in clouds enriched by Pop III SNe (G. Chiaki et al. 2018; G. Chiaki & J. H. Wise 2019; G. Chiaki et al. 2020). In order to reproduce the elemental abundances of EMP stars, mixing and fallback are introduced in SN nucleosynthesis (H. Umeda & K. Nomoto 2003; N. Tominaga et al. 2014). These processes can significantly suppress the production of grains made of heavier elements than O.

2. Methods

We use a one-dimensional spherically symmetric stellar and explosive nucleosynthesis model calculated by N. Tominaga et al. (2007). The electron fraction Y_e in the incomplete Si-burning region is set to be 0.4997 (C. Kobayashi et al. 2006). The model includes reaction networks of 280 isotopes up to ^{79}Br. We then calculate the final abundance of isotopes, considering the decay of radioactive isotopes. Summing up the isotopes with the same atomic number at a given radius, we obtain the radial distribution of elemental abundances as the initial condition of our molecule/dust formation calculations.

The density and temperature evolutions of SN ejecta are calculated in detail, at each mass coordinate in the expanding ejecta, using the method developed by K. Iwamoto et al. (2000). Assuming a homologous expansion, the density $\rho(M_r)$ at each mass coordinate M_r decreases as $\rho(M_r) \propto t^{-3}$ as a function of time t. We include adiabatic expansion cooling and ^{56}Ni decay heating. The model also solves radiation transfer, and the gas loses and gains thermal energy through thermal radiation and photon absorption, respectively.

At each mass coordinate, our model solves the formation/dissociation of eight diatomic molecular species: SiC, CO, SiS, SiO, O_2, S_2, CS, and SO. We calculate the radiative association reaction rates with the empirical Arrhenius form. Dissociation is induced by the collision with all gas-phase species whose kinetic energy exceeds the binding energy of the dissociating molecules. We calculate the reaction cross sections from the geometrical radii of impactors.

Our model simultaneously solves the nucleation and growth for 12 grain species: C, Si, SiC, Fe, FeS, FeO, Fe_3O_4, Al_2O_3, $MgSiO_3$, Mg_2SiO_4, SiO_2, and MgO, using the non-steady-state classical nucleation theory (CNT) of N13 (see also R. Schneider & R. Maiolino 2023, for a review).[8] In this model, we assume that grains form through the reactions presented in Table 2 of T. Nozawa et al. (2003). For instance, alumina (Al_2O_3) is produced by the reaction

$$2\mathrm{Al(g)} + 3\mathrm{O(g)} \rightarrow \mathrm{Al_2O_3(s)}, \quad (1)$$

where (g) and (s) denote the gas and solid phase, respectively. Through the reaction, in a mass coordinate with a sufficient abundance of Al and O, these atoms can directly condense into alumina grains when the supersaturation rate drops below $\sim$1 (for more details, see Section 4). Also, here we adopt the so-called a "key-species" approach, where the reaction rate is limited by the minimum collision rate among reactant species (key species). After the reaction, the abundance of other reactants decreases by the stoichiometric number times the decrement of the key species.

In this work, we use a hypernova model with a progenitor mass of $M_{\mathrm{PopIII}} = 25\,M_\odot$ and explosion energy of 10 B (1 B $= 10^{51}$ erg). M. N. Ishigaki et al. (2018) compared the elemental abundances of 202 EMP stars with the yield of Pop III SNe with different M_{PopIII} and E_{SN}. They found that the majority of the EMP stars (55%) can be fitted with the Pop III hypernova model with $M_{\mathrm{PopIII}} = 25\,M_\odot$ and $E_{\mathrm{SN}} = 10$ B. We also test the case with $E_{\mathrm{SN}} = 1$ B (Section 3.4).

Using the SN model, we run the following four calculations of dust synthesis as summarized in Table 1. In the first two runs, we use a mass cut for $M_{^{56}\mathrm{Ni}} = 0.07\,M_\odot$, by setting a remnant mass $M_{\mathrm{rem}} = 2.39\,M_\odot$. The dotted curves in Figure 1(a) show the mass fraction of elements (after decays) as a function of mass coordinate in the SN ejecta. Heavier elements, such as iron, are synthesized in the inner region. The region below the plotted range ($M < 2.39 M_\odot$) is not ejected and falls into the remnant, in the mass-cut model M25E10. The blue line in Figure 1(b) shows the elemental abundances of the SN ejecta relative to C. With this mass-cut model, we run the following two calculations with different chemical processes to demonstrate the impact of molecule formation. In the first case, C and Si are initially in the atomic form, and both molecule and dust formation are solved with our code (`M25E10`). In the second case, we assume a simplified model, where C and Si atoms are depleted into CO and SiO, respectively, from the beginning, and the abundances of these molecules are fixed throughout the calculation (`M25E10mol.fix`).

In the other two runs, we use more realistic SN models considering two mixing/fallback cases that correspond to the two major classifications of observed EMP stars: one with solar-like ("normal") elemental abundance ratios (C-normal stars) and the other with carbon enhancement of [C/Fe] > 0.7 (C-enhanced metal-poor or CEMP stars; T. C. Beers & N. Christlieb 2005; G. Chiaki et al. 2017). Here, we adopt a

[6] In this work, we define "molecules" as diatomic species that are not locked up into grains.

[7] $[\mathrm{A/B}] = \log(n_\mathrm{A}/n_\mathrm{B}) - \log(n_\mathrm{A}/n_\mathrm{B})_\odot$, where n_X is the number abundance of a element X. Here, we use the solar elemental abundance presented by M. Asplund et al. (2009).

[8] Although the UV bump in the galaxy JADES-GS-z6-0 is the sign of graphite, we consider carbonaceous grains as monoatomic, amorphous carbon grains in this work.

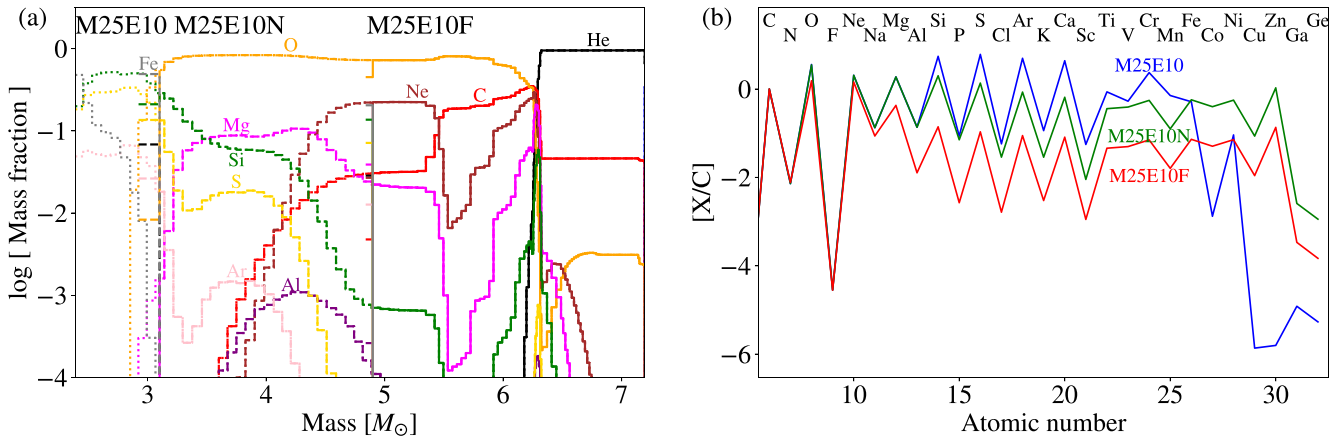

Figure 1. (Panel (a)) Mass fraction of elements as a function of enclosed mass in the He core (outside the remnant) for a Pop III hypernova with a mass of 25 $M_\odot$ and explosion energy 10 B. The dotted, dashed, and solid curves show the results of the model without mixing/fallback (`M25E10`), and the normal (`M25E10N`) and faint (`M25E10F`) hypernova models, which respectively reproduce the elemental abundances of C-normal and C-enhanced metal-poor stars. (Panel (b)) Number fraction of elements from B to Ge relative to C in the models `M25E10` (blue), `M25E10N` (green), and `M25E10F` (red).

Table 1
Input Parameters and Dust Masses of Pop III SN Models

Model	$M_{\rm pr}$ ($M_\odot$)	$E_{\rm SN}$ (B)	$M_{\rm cut}$ ($M_\odot$)	$M_{\rm mix}$ ($M_\odot$)	$\log f_{\rm ej}$	$M_{\rm rem}$ ($M_\odot$)	$M_{^{56}\rm Ni}$ ($M_\odot$)	$t_{\rm fin}$ (days)	$M_{\rm C}$ ($M_\odot$)	$M_{\rm si}$ ($M_\odot$)	$M_{\rm Mg_2SiO_4}$ ($M_\odot$)	$M_{\rm d}$ ($M_\odot$)
(1)	(2)	(3)	(4)	(5)	(6)	(7)	(8)	(9)	(10)	(11)	(12)	(13)
`M25E10`	25	10	1.69	2.39	$-\infty$	2.39	7.00×10^{-2}	840	8.45×10^{-2}	0.196	0.260	0.926
`M25E10mol.fix`	25	10	1.69	2.39	$-\infty$	2.39	7.00×10^{-2}	840	5.77×10^{-2}	0.270	0.260	0.985
`M25E10N`	25	10	1.69	3.1	−0.9	2.92	8.41×10^{-2}	713	8.70×10^{-2}	4.43×10^{-2}	0.259	0.706
`M25E10F`	25	10	1.69	4.9	−1.8	4.85	1.01×10^{-2}	503	6.78×10^{-2}	2.71×10^{-3}	9.98×10^{-3}	0.139
`M25E1`	25	1	1.69	1.89	$-\infty$	1.89	7.00×10^{-2}	1118	4.44×10^{-2}	0.108	0.145	0.636
`M25E1mol.fix`	25	1	1.69	1.89	$-\infty$	1.89	7.00×10^{-2}	1118	4.15×10^{-2}	0.188	0.153	0.674
`M25E1F`	25	1	1.69	5.4	−2.2	5.38	1.54×10^{-3}	767	4.19×10^{-2}	$<10^{-5}$	$<10^{-5}$	4.83×10^{-2}

Notes. (1) ID of run. (2) Progenitor mass. (3) Explosion energy. (4) Initial mass cut. (5) Outer boundary of mixing. (6) Ejection fraction. (7) Remnant mass. (8) Ejected ^{56}Ni mass. (9) Time when we terminate the calculations, in days. (10–12) Masses of C, Si, and Mg_2SiO_4 (silicate) grains. (13) Total dust mass.

jet-like SN explosion model described with three parameters, which are determined from the observations: the initial mass cut $M_{\rm cut}$, the fraction $f_{\rm ej}$ of gas ejected in the polar directions, and the mass $M_{\rm mix}$ that is subject to mixing (N. Tominaga 2009). These parameters give the corresponding remnant mass $M_{\rm rem} = M_{\rm cut} + (1 - f_{\rm ej})(M_{\rm mix} - M_{\rm cut})$.

In the former (called `M25E10N`), we set a moderate $M_{\rm mix} = 3.1\,M_\odot$ and $\log f_{\rm ej} = -0.9$ to reproduce the elemental abundances of a C-normal star SMSS J093209.41−003435.8. In the latter (`M25E10F`), we set a large $M_{\rm mix} = 4.9$ and small $\log f_{\rm ej} = 1.8$ to reproduce those of a C-enhanced star SMSS J005953.98−594329.9 (M. N. Ishigaki et al. 2018). The dashed and solid curves in Figure 1(a) show the radial profile of elemental abundances for `M25E10N` and `M25E10F`, respectively, where the inner part of ejecta ($M_{\rm r} < 2.92$ and $4.85\,M_\odot$) falls back on to the remnant. The resultant yields are shown Figure 1(b) with green and red lines, respectively. The latter type of SNe can eject Fe-deficient or relatively C-rich materials, and is used to reproduce the elemental abundances of C-enhanced metal-poor stars. This SN type is called a "faint" SN due to its small $M_{^{56}\rm Ni}$. In these mixing/fallback models, we solve molecule formation reactions together with dust formation.

In our code, we first calculate the temperature evolution in ejecta until 2000 days after explosion. Using the results, we start the dust formation calculations when the temperature of at least one radius bin falls below 10^4 K, and terminate the calculations when the temperature of all bins falls below 300 K, as shown in the ninth column of Table 1. Although radiative cooling due to newly forming molecules can affect the hydrodynamical evolution of ejecta (S. Liljegren et al. 2020), we do not take it into account in this work, to isolate the effect of molecule formation.

3. Results

We can successfully calculate molecule and dust formation in the ejecta fully self-consistently, as shown in Figure 2. Table 1 gives a summary of the model parameters and results. In this section, we analyze the produced dust mass and its composition in detail.

3.1. Molecule and Dust Formation

We first present the results in the model `M25E10`. Figure 2 shows the evolution of (a) temperature and (b) species abundances at an enclosed mass of $M_{\rm r} = 6.2\,M_\odot$ (C layer).

At time $t = 80$ days, some of the C atoms (red dotted) are oxidized into CO molecules (orange dashed). At $t = 177$ days, where the gas temperature drops below ∼1700 K, which is comparable to the sublimation temperature, C grains (blue solid) start to form from the remaining C atoms.[9] Figure 3(a) shows the number fraction of chemical species as a function of M_r. C grains (blue solid) form at a range of $M_r = 5.5$–$6.3\,M_\odot$, and in total, $8.45 \times 10^{-2}\,M_\odot$ C grains are ejected.

The other species form in different layers with different elemental abundances (Figure 3). Metallic Si (yellow solid) forms mainly in the Si–S–Fe layer ($M_r = 2.5$–$3.0\,M_\odot$). A fraction of Si atoms that are not depleted into SiS molecules can condense into metallic Si grains. In the O–Si–S layer ($M_r = 3.0$–$3.2\,M_\odot$), SiO_2 is the dominant grain species. Mg_2SiO_4 (green solid) forms mainly in the O–Si–Mg and O–Mg–Si layers ($M_r = 3.2$–$4.4\,M_\odot$).

We show the masses of the major dust species in Table 2 (a). The dominant species are metallic Si, Mg_2SiO_4, and SiO_2. In total, $\sim 1\,M_\odot$ of dust is produced in `M25E10`. Table 2 (b) shows the mass fraction of elements finally depleted into grains. We find that ∼30% of C nuclei are locked up into C grains, while almost 100% of Mg, Al, and Fe are depleted into grains. In total, 23.4% of metals are locked up into grains.

3.2. The Importance of Molecule Formation

In the simple chemistry model, `M25E10mol.fix`, the total dust mass ($M_d = 0.985\,M_\odot$) is almost the same as that of `M25E10mol`, but the masses of several species, such as C and Si, are significantly different. The C grain mass is underestimated by ∼30%, compared with `M25E10`. We can clearly see that the C grain abundance is smaller in the inner region of the C layer ($M_r = 5.5$–$6.2\,M_\odot$), comparing Figures 3(a) and (b). To interpret this, we compare the evolution of species abundances for `M25E10` and `M25E10mol.fix` at $M_r = 6.2\,M_\odot$ (Figures 2(b) and (c)). In this layer, the C abundance is only slightly larger than that of O, and thus only a small fraction of C atoms (∼0.03) are available to condense in `M25E10mol.fix` (panel (c)). In `M25E10` (panel (b)), C and O are initially in the atomic form, and CO molecules form at a timescale comparable to grain formation. Therefore, a larger amount of C atoms (∼0.2) remain just before C grain formation.

Metallic Si mass is overestimated in `M25E10mol.fix` by ∼40%, compared with `M25E10`. In `M25E10mol.fix`, where we consider only SiO molecule formation, all Si can remain in the atomic form because O is not synthesized in the Si-rich layer (Figure 1). In `M25E10`, since we include the formation of molecules other than SiO, some of the Si has been depleted into SiS molecules before Si grain formation.

3.3. Mixing/Fallback

In the mass-cut model with $M_{^{56}\mathrm{Ni}} = 0.07\,M_\odot$, the mass ratio of C grains to silicates is small (∼0.325) because the ejecta are overall O-rich. In the extinction curve derived from the grain composition, the observed UV bump would not appear. In mixing/fallback models, however, only silicate grain mass is expected to be suppressed.

In `M25E10N`, mixing/fallback can reduce the total dust mass down to $0.706\,M_\odot$, compared with `M25E10`, due to the fallback of inner materials (Table 1). However, the C grain mass is almost unchanged ($8.70 \times 10^{-3}\,M_\odot$), because the outer C-layer is not affected by mixing/fallback. The Fe–Si–S and Si–S–Fe layers ($M_r < 3.0\,M_\odot$) fall back (dashed curves in Figure 1), which suppresses the mass of Si and FeS grains by ∼50%. However, silicate mass is still high ($0.259\,M_\odot$), and the ratio of C grains to silicates is only ∼0.335. In this case, the

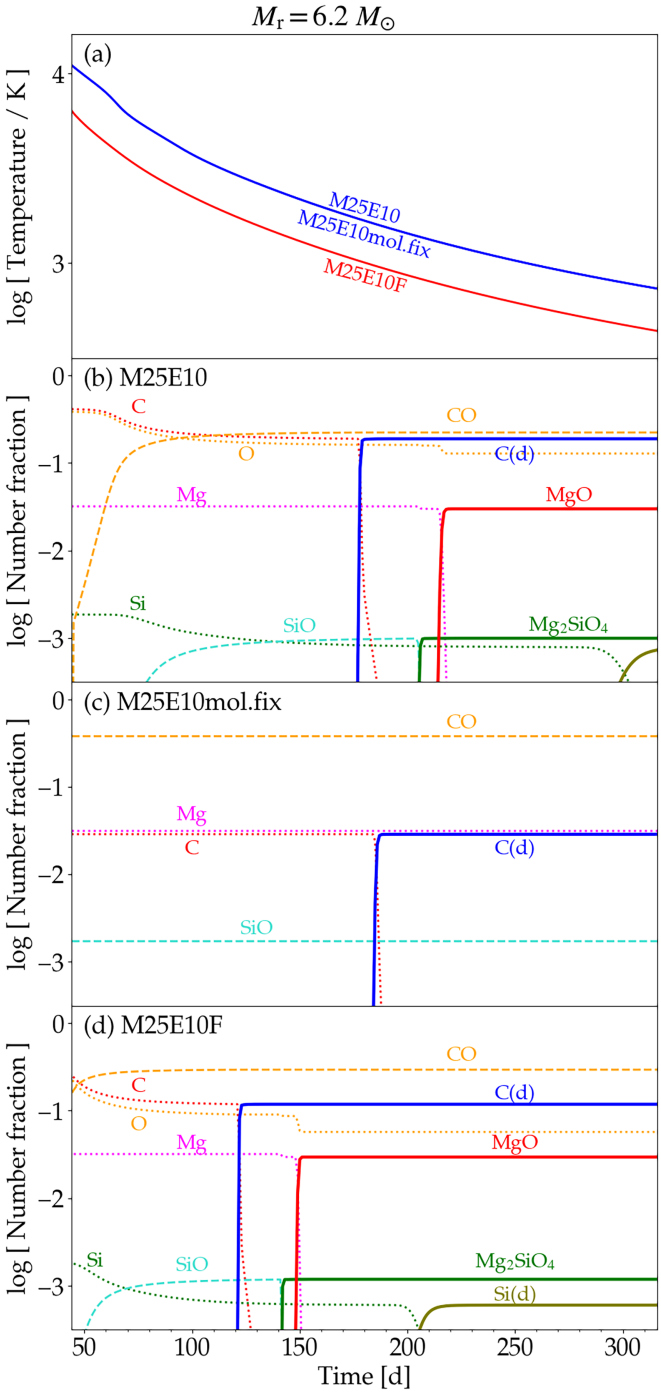

Figure 2. Time evolution of (a) the gas temperature and ((b)–(d)) number abundance of chemical species at an enclosed mass of $M_r = 6.2\,M_\odot$. In panel (a), the blue and red curves show the results for `M25E10` and `M25E10F`, respectively. The curve for `M25E10mol.fix` is overlapped with that of `M25E10` because we use the same SN model. The other panels indicate atomic (dotted), molecular (dashed), and grain (solid) species for (b) `M25E10`, (c) `M25E10mol.fix`, and (d) `M25E10F`. We do not show the result for `M25E10N`, because it is almost the same as that for `M25E10`.

[9] In Figure 2, the blue solid curve shows the number fraction of C nuclei locked up into C grains.

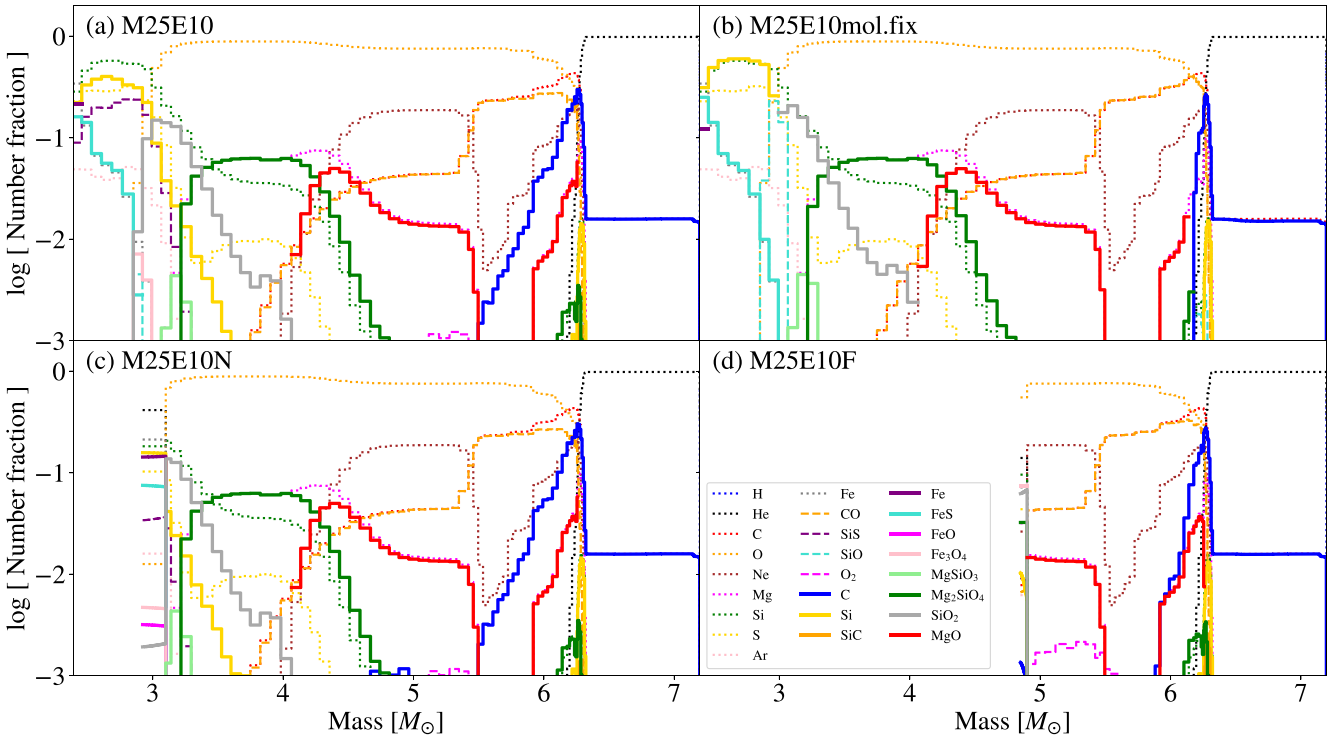

Figure 3. Number abundance of chemical species as a function of enclosed mass for (a) `M25E10`, (b) `M25E10mol.fix`, (c) `M25E10N`, and (d) `M25E10F`. The dotted curves indicate the initial abundances of elements, and the dashed and solid curves indicate the final abundances of molecules and grains, respectively.

Table 2
Metal and Grain Production in `M25E10`

(a) Dust mass in units of $M_\odot$

C	Si	Fe	FeS	Fe_3O_4	Al_2O_3	$MgSiO_3$	Mg_2SiO_4	SiO_2	MgO	Total
8.45×10^{-2}	0.196	2.05×10^{-2}	9.73×10^{-2}	2.14×10^{-3}	1.69×10^{-3}	3.81×10^{-3}	0.260	0.169	9.17×10^{-2}	0.926

(b) Fraction of elements depleted into grains

C	O	Mg	Al	Si	S	Fe	Total
0.304	0.103	0.939	1.000	0.738	0.153	1.000	0.234

interstellar medium enriched by this SN still would not show the remarkable UV bump.

In `M25E10F`, the inner region, even within the O–Ne–Mg layer ($M_r < 4.85\,M_\odot$), falls back. Accordingly, the masses of Fe-, Si-, Mg-, Al-, and O-bearing species are reduced by several orders of magnitude (Figure 3(d)). On the other hand, the mass of C grains produced is $6.78 \times 10^{-2}\,M_\odot$, only ∼20% lower than in `M25E10`.

The C grain production is not significantly changed, because the C layer ($M_r \sim 6\,M_\odot$) is not affected by mixing/fallback. The slight decrease by ∼20% is due to the temperature evolution of the ejecta (Figure 2(d)). In this faint SN model, the mass of the main heat source, ^{56}Ni, is smaller ($M_{^{56}\mathrm{Ni}} = 1.01 \times 10^{-2}\,M_\odot$) than those of the other models. Since the gas temperature is lower than in `M25E10` by ∼20%, CO molecule formation is slightly enhanced. Then, available C atoms are reduced, and thus the mass of C grains is slightly suppressed. The mass ratio of C grains to silicates is still high (∼7), which could explain the observed spectral features of galaxy JADES-GS-z6-0.

3.4. Lower Explosion Energy Case

So far, we have set the explosion energy to be $E_{\rm SN} = 10$ B. The properties of forming grains may be altered by the explosion energy. We also test the case with a lower explosion energy, $E_{\rm SN} = 1$ B, keeping the other parameters the same as in Table 1. With $0.07\,M_\odot^{56}$ Ni, molecule formation is self-consistently solved in `M25E1` but not in `M25E1mol.fix`. Finally, we consider a mixing/fallback model, `M25E1F`, with $M_{\rm mix} = 5.4\,M_\odot$ and $\log f_{\rm ej} = -2.2$ that can reproduce the elemental abundance of a C-enhanced star, SDSS J014036.21 +234458.1.

As summerized in Table 1, the dust mass for `M25E1` ($0.636\,M_\odot$) is smaller than in `M25E10`. This is because the synthesized metal mass is smaller for the lower explosion energy. We find that the C grain mass is almost the same between `M25E1` and `M25E1mol.fix`, unlike the $E_{\rm SN} = 10$ B case. This is because the grain formation timescale is longer, relative to the CO molecule formation timescale, than in `M25E10`. With the lower explosion energy, ejecta expand

more slowly, and the gas temperature falls below the sublimation temperature later.

For M25E1F, the dust mass ($4.27 \times 10^{-2}\,M_\odot$) is smaller than in M25E1 ($\sim 0.6\,M_\odot$) because of the fallback. The Si and Mg_2SiO_4 grain masses are much smaller than in M25E1, while the C grain mass ($4.19 \times 10^{-2}\,M_\odot$) is almost unchanged from M25E1 ($4.44 \times 10^{-2}\,M_\odot$). These tendencies are the same as in the $E_{\rm SN} = 10$ B case, and thus we can conclude that both faint SNe and faint hypernovae can cause the remarkable UV bump.

4. Discussion

Although our dust synthesis code is unique, with its self-consistent treatment of molecule formation, our results can be compared with other studies as follows. E. S. Brooker et al. (2022) studied dust formation with the same formulation as in our work, but without molecule formation and with different initial metallicities of 10^{-4}–$10^{-1}\,Z_\odot$. Since the metals synthesized in the pre-SN phase are dominant over the initially existing metals, the initial metallicity should have only a minor effect on the dust mass. They run simulations with a progenitor mass of $25\,M_\odot$ with $\sim$10 B and $\sim$1 B, which are comparable to our models without molecule formation. With 10B, the C grain mass in our M25E10mol.fix model ($5.77 \times 10^{-2}\,M_\odot$) is a factor of four larger than the result of their M25bE9.73 model ($1.39 \times 10^{-2}\,M_\odot$). The silicate mass in our M25E10 model ($0.260\,M_\odot$) is very similar to their result ($0.256\,M_\odot$). With 1 B, the C grain mass in our M25E1mol.fix model ($4.15 \times 10^{-2}\,M_\odot$) is a factor of three larger than the result of their M25d3E0.92 model ($1.37 \times 10^{-2}\,M_\odot$). The silicate mass obtained by our study ($0.153\,M_\odot$) is similar to their result ($0.208\,M_\odot$). Therefore, the carbonaceous dust mass is larger in our models than in E. S. Brooker et al. (2022). This is because the abundance of C atoms in our work is smaller than in their model, in the C-rich layer.

These studies of dust formation are based on the CNT-based approach as well as this work. Another approach is to compute non-equilibrium chemistry related to the formation of molecules and dust clusters (A. Sarangi & I. Cherchneff 2013; C. Biscaro & I. Cherchneff 2014). The grain mass with this approach is smaller than with our CNT approach by a factor of $\sim$10. This may be because high-energy ions destroy the reactant molecules. For example, in their model, Al_2O_3 grains form through the reaction including AlO molecules that are not included in our model (Equation (1)). The molecules tend to be quickly destroyed by Ne^+ ions in the gas. It is necessary to carefully compare these approaches in further detail.

There are longer-term physical processes that can affect the dust mass produced by an SN. First of all, if SN ejecta interact with the dense circumstellar medium (CSM), dust can form again in the interaction region at later time ($\sim$10 yr; M. Shahbandeh et al. 2025). In this work, dust formation is followed only until $\sim$1000 days, and additional dust production in the CSM is not considered. Note, however, that our model can be applied to the CSM interaction once its physical condition is specified. After that, reverse shocks propagating in ejecta are supposed to destroy a significant amount of dust produced by an SN $\sim 10^4$ yr after the explosion, which can reduce the final dust mass released from the SN (S. Bianchi & R. Schneider 2007; T. Nozawa et al. 2007).

Second, dust mass could be enhanced by a clumpy structure of ejecta, although spherically symmetric ejecta structure is assumed in this paper. A. Sarangi & I. Cherchneff (2015) found that the formation of large grains ($\gtrsim 0.1\,\mu$m) is favored in clumpy ejecta, and the mass of several grain species, such as metallic silicon, can be enhanced. It would be interesting to test grain formation with clumpy ejecta structure, in particular in HN cases, which might increase the metallic silicon mass and make it the dominant species.

Finally, in this paper, we focused on the mass fraction of carbonaceous grains produced by a Pop III SN and have not calculated their sizes. The size distribution is crucial to the cooling efficiency of star-forming clouds (G. Chiaki & J. H. Wise 2019; G. Chiaki et al. 2020) as well as the extinction curves of galaxies (Y. Dubois et al. 2024), which we hope to predict in our future works.

5. Conclusion

Recent JWST observations have revealed the spectral feature ("UV bump") of carbonaceous grains in the distant galaxy JADES-GS-z6-0 at $z = 6.7$ (J. Witstok et al. 2023b). It is puzzling how the galaxy could have acquired C grains in the very early Universe. In this paper, we present the first results of our state-of-the-art dust synthesis code to study dust formation in Pop III SN ejecta, including molecule formation and mixing/fallback effects, fully self-consistently.

First, we find that the inclusion of molecule formation reactions significantly affects grain formation. It is an over-simplification to assume that all available C and Si deplete into CO and SiO initially, as in previous works. C grain mass is underestimated by $\sim$40%, compared to our fiducial model where both molecule and dust formation reactions are solved self-consistently. This is because the timescales for CO molecular formation and C grain formation are comparable, and some of the C atoms can remain just before C grain formation. Larger dust production per SN might help explain the large dust mass observed with ALMA. However, a large amount of silicates is produced at the same time, which is likely to hide the UV bump.

Second, we find that the mixing/fallback of ejecta remarkably affects the dust composition. We consider two models that reproduce the elemental abundances of descendant C-normal and C-enhanced metal-poor stars (M25E10N and M25E10F, respectively). For the faint SN model, although the total dust amount is 85% smaller, the C grain mass ($6.78 \times 10^{-2}\,M_\odot$) is only 20% smaller than in the hypernova model, resulting in a carbonaceous to silicate grain ratio of $\sim$0.3. This may be a clue to explain the remarkable UV bump in a high-redshift galaxy (J. Witstok et al. 2023b). We conclude that faint SNe may be C grain factories in the early Universe.

This study is the very first step to uncover the cosmic dust formation history. In this work, we showed the dust masses only for $M_{\rm PopIII} = 25\,M_\odot$ and explosion energies $E_{\rm SN} = 1$ and 10 B. For higher $M_{\rm PopIII}$, the dust mass would be larger because the synthesized metal mass is larger (T. Nozawa et al. 2003). For higher $E_{\rm SN}$, the more abundant O is synthesized. Therefore, we can expect the masses of oxidized grains, such as silicates, silica, and alumina, to increase. In future works, we will study dust formation in ejecta of various progenitors, ideally taking account of the multidimensional and clumpy effects on the additional formation and destruction in the CSM (Section 4). From these studies, we will eventually build a

comprehensive GCE model to self-consistently follow the cosmic evolution of dust and metals.

Acknowledgments

We are grateful to T. Nozawa for his crucial contributions to this research. We thank M. Ishigaki, T. Hosokawa, R. Matsukoba, and K. Omukai for discussions. This work was supported by JSPS KAKENHI grant No. 24H00027. C.K. acknowledges funding from the UK Science and Technology Facility Council through grant ST/R000905/1, ST/V000632/1, ST/Y001443/1. The work was also funded by a Leverhulme Trust Research Project Grant on "Birth of Elements."

Software: MATPLOTLIB(J. D. Hunter 2007).

Data Availability

Two SN models for $25M_{\odot}$ models with explosion energies of 1 and 10 B are available on Zenodo at DOI: 10.5281/zenodo.19364861. Each file provides the masses of the major element nuclei, the mass fraction of elements depleted onto dust grains, and the masses of molecules and dust grains at the end of the model simulation.

ORCID iDs

Gen Chiaki https://orcid.org/0000-0001-6246-2866
Chiaki Kobayashi https://orcid.org/0000-0002-4343-0487
Nozomu Tominaga https://orcid.org/0000-0001-8537-3153

References

Asplund, M., Grevesse, N., Sauval, A. J., & Scott, P. 2009, ARA&A, 47, 481
Beers, T. C., & Christlieb, N. 2005, ARA&A, 43, 531
Bianchi, S., & Schneider, R. 2007, MNRAS, 378, 973
Biscaro, C., & Cherchneff, I. 2014, A&A, 564, A25
Brooker, E. S., Stangl, S. M., Mauney, C. M., & Fryer, C. L. 2022, ApJ, 931, 85
Bunker, A. J., Saxena, A., Cameron, A. J., et al. 2023, A&A, 677, A88
Carniani, S., Hainline, K., D'Eugenio, F., et al. 2024, Natur, 633, 318
Chiaki, G., Susa, H., & Hirano, S. 2018, MNRAS, 475, 4378
Chiaki, G., Tominaga, N., & Nozawa, T. 2017, MNRAS, 472, L115
Chiaki, G., & Wise, J. H. 2019, MNRAS, 482, 3933
Chiaki, G., Wise, J. H., Marassi, S., et al. 2020, MNRAS, 497, 3149
Choplin, A., Tominaga, N., & Ishigaki, M. N. 2019, A&A, 632, A62
Dayal, P., Ferrara, A., Sommovigo, L., et al. 2022, MNRAS, 512, 989
D'Eugenio, F., Maiolino, R., Carniani, S., et al. 2023, A&A, 689, A152
Dubois, Y., Rodríguez Montero, F., Guerra, C., et al. 2024, A&A, 687, A240
Hunter, J. D. 2007, CSE, 9, 90
Ishigaki, M. N., Tominaga, N., Kobayashi, C., & Nomoto, K. 2018, ApJ, 857, 46
Iwamoto, K., Nakamura, T., Nomoto, K., et al. 2000, ApJ, 534, 660
Kobayashi, C., Karakas, A. I., & Lugaro, M. 2020, ApJ, 900, 179
Kobayashi, C., Umeda, H., Nomoto, K., Tominaga, N., & Ohkubo, T. 2006, ApJ, 653, 1145
Liljegren, S., Jerkstrand, A., & Grumer, J. 2020, A&A, 642, A135
Marassi, S., Chiaki, G., Schneider, R., et al. 2014, ApJ, 794, 100
Marassi, S., Schneider, R., Limongi, M., et al. 2015, MNRAS, 454, 4250
Marassi, S., Schneider, R., Limongi, M., et al. 2019, MNRAS, 484, 2587
Nozawa, T., & Fukugita, M. 2013, ApJ, 770, 27
Nozawa, T., & Kozasa, T. 2013, ApJ, 776, 24
Nozawa, T., Kozasa, T., Habe, A., et al. 2007, ApJ, 666, 955
Nozawa, T., Kozasa, T., Umeda, H., Maeda, K., & Nomoto, K. 2003, ApJ, 598, 785
Sarangi, A., & Cherchneff, I. 2013, ApJ, 776, 107
Sarangi, A., & Cherchneff, I. 2015, A&A, 575, A95
Schneider, R., Ferrara, A., Salvaterra, R., Omukai, K., & Bromm, V. 2003, Natur, 422, 869
Schneider, R., & Maiolino, R. 2023, A&ARv, 32, 2
Shahbandeh, M., Fox, O. D., Temim, T., et al. 2025, ApJ, 985, 262
Tamura, Y., Mawatari, K., Hashimoto, T., et al. 2019, ApJ, 874, 27
Todini, P., & Ferrara, A. 2001, MNRAS, 325, 726
Tominaga, N. 2009, ApJ, 690, 526
Tominaga, N., Iwamoto, N., & Nomoto, K. 2014, ApJ, 785, 98
Tominaga, N., Umeda, H., & Nomoto, K. 2007, ApJ, 660, 516
Umeda, H., & Nomoto, K. 2003, Natur, 422, 871
Umeda, H., Nomoto, K., & Nakamura, T. 2000, in The First Stars: Proceedings of the MPA/ESO Workshop, ed. A. Weiss, T. G. Abel, & V. Hill (Springer-Verlag), 150
Watson, D., Christensen, L., Knudsen, K. K., et al. 2015, Natur, 519, 327
Witstok, J., Jones, G. C., Maiolino, R., Smit, R., & Schneider, R. 2023a, MNRAS, 523, 3119
Witstok, J., Shivaei, I., Smit, R., et al. 2023b, Natur, 621, 267
Witstok, J., Smit, R., Maiolino, R., et al. 2022, MNRAS, 515, 1751